journal

Spinel Coumpounds: Structure and Property Relations

J. Am. Ceram. Soc., **82** [12] 3279–92 (1999)

Structure of Spinel

Kurt E. Sickafus*,† and John M. Wills

Los Alamos National Laboratory, Los Alamos, New Mexico 87545

Norman W. Grimes*

Aston University, Birmingham B4 7ET, England

This paper reviews the crystal structure of compounds with the general formula AB_2X_4, which crystallize with the same atomic structure as the mineral spinel, $MgAl_2O_4$. Three degrees of freedom associated with the detailed atomic arrangements of spinels are considered here: (i) the lattice parameter, *a*; (ii) the anion parameter, *u*; and (iii) the cation inversion parameter, *i*. Oxide spinels are used as examples to explore the interrelationships between these parameters.

I. Introduction

SEVERAL binary chalcogenides that have the general formula AB_2X_4 (A and B are cations; X is an anion (O, S, Se, Te)) crystallize with the same structure as the mineral spinel, $MgAl_2O_4$, which is the parent compound in this group. Many spinels exhibit remarkable electrical, magnetic, and other physical characteristics.[1] This paper examines the structure behind these unique materials.

II. Crystal Structure

The crystal structure of spinel was determined independently by Bragg[2] and Nishikawa.[3] The majority of spinel compounds belong to the space group $Fd3m$ ($F^4_{1/d}\bar{3}_{2/m}$; O^7_h; No. 227 in the International Tables[4]). The primitive tetrahedral unit cell of spinel is illustrated in Fig. 1. This cell consists of two molecular AB_2X_4 units and is represented by two octants in Fig. 1, with atomic positions indicated in the diagram. Four primitive unit cells, arranged as shown in Fig. 1, combine to form the conventional, cubic unit cell of spinel. Consequently, there are $Z = 8$ formula units per cubic unit cell, each of which consist of 32 anions and 24 cations, for a total of 56 atoms. The Bravais lattice of the conventional unit cell is face-centered cubic (fcc); the basis consists of two formula units.

The anion sublattice is arranged in a pseudo-cubic close-packed (ccp) spatial arrangement, although some spinels possess almost-ideal ccp anion sublattices. The repeat unit of the conventional unit cell is twice that of the anion lattice (the latter is one octant in Fig. 1). As a consequence, the spinel lattice parameters (a) are large. In natural $MgAl_2O_4$, for instance, $a = 0.80898(9)$ nm.[5]

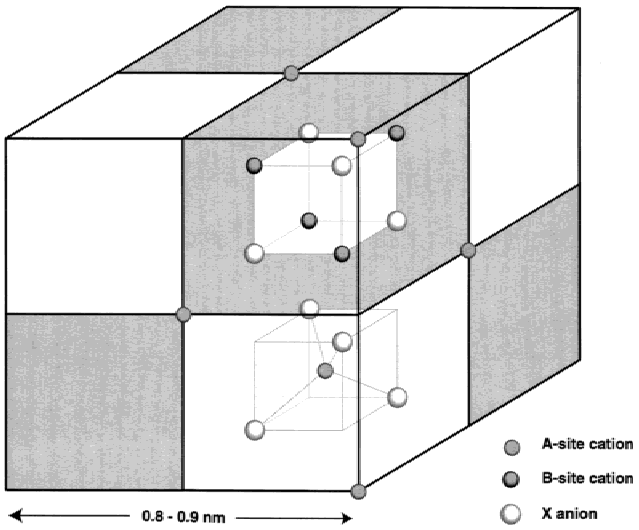

Fig. 1. Primitive tetragonal and conventional cubic unit cells of spinel. The primitive cell consists of two octants of the cubic unit cell. Atom positions are shown for the primitive unit cell only; however, the atomic positions denoted in the primitive cell repeat with the pattern indicated by shading in the other octants. One A-site in the primitive cell is not visible in the drawing; it is on the center of the base of the cubic unit cell. The lattice-parameter range ($a = 0.8$–0.9 nm) is approximately the range corresponding to oxide spinels.

There are 96 interstices between the anions in the cubic unit cell; however, in AB_2X_4 compounds, only 24 are occupied by cations. Of the 64 tetrahedral interstices that exist between the anions, 8 are occupied by cations. The remaining 16 cations occupy half of the 32 octahedral interstices. The tetrahedrally coordinated cations form a diamond cubic sublattice with a repeat unit equal to the lattice parameter. The periodicity associated with the sublattice of octahedrally coordinated cations also is equal to a. The overall cation sublattice possesses the same structure as the $MgCu_2$ C15 Laves phase.[6]

Description of the atomic positions in spinel is dependent on the choice of setting for the origin in the $Fd3m$ space group. Two different equipoints with point symmetries $\bar{4}3m$ and $\bar{3}m$ are possible choices for the unit-cell origin. Moreover, the origin can be assigned to either a vacant site or an occupied lattice site. Table I lists the arrangement of lattice sites along the unit-cell body diagonal for four possible choices of origin. The equipoints for the various lattice sites are denoted using Wyckoff notation.[7] In Table I and throughout this paper, tetrahedral cation sites are called A-sites, whereas octahedral cation sites are called B-sites (this convention often is used among chemists and physicists; however, mineralogists define spinels as A_2BO_4 compounds and all cation-site definitions are reversed). The conventional choices for the unit-cell origin in spinel are either $\bar{4}3m$ on an A-site cation or $\bar{3}m$ on an octahedral vacancy

H. U. Anderson—contributing editor

Manuscript No. 189665. Received December 28, 1998; approved October 13, 1999.
This work was sponsored by the U.S. Dept. of Energy, Office of Basic Energy Sciences, Division of Materials Sciences, and a research and development grant directed by Los Alamos National Laboratory.
Presented at the 100th Annual Meeting of The American Ceramic Society, Cincinnati, OH, May 5, 1998 (Basic Science Division Special Session on Spinel Compounds: Structure and Property Relations, Paper No, BS13-003-98).
*Member, American Ceramic Society.
†Author to whom correspondence should be addressed.

Table I. Lattice Sites along the Cube Body Diagonal in the Ideal Conventional Unit Cell of Spinel

Fractional coordinates along body diagonal of unit cell	Origin at $\bar{4}3m$			Origin at $\bar{3}m$		
	Equipoint†	Origin on A-site	Origin on tetrahedral vacancy	Equipoint†	Origin on B-site	Origin on octahedral vacancy
0,0,0	8a	A-site cation	Tetrahedral vacancy	16c	B-site cation	Octahedral vacancy
⅛,⅛,⅛	16c	Octahedral vacancy	B-site cation	8a	Tetrahedral vacancy	A-site cation
¼,¼,¼	8a	A-site cation	Tetrahedral vacancy	32e	Anion X	Anion X
⅜,⅜,⅜	32e	Anion X	Anion X	8b	A-site cation	Tetrahedral vacancy
½,½,½	8b	Tetrahedral vacancy	A-site cation	16d	Octahedral vacancy	B-site cation
⅝,⅝,⅝	16d	B-site cation	Octahedral vacancy	8b	A-site cation	Tetrahedral vacancy
¾,¾,¾	8b	Tetrahedral vacancy	A-site cation	32e	Anion X	Anion X
⅞,⅞,⅞	32e	Anion X	Anion X	8a	Tetrahedral vacancy	A-site cation

†Wycoff notation.

(the latter is an inversion center). Table II lists the fractional coordinates of atoms in the unit cell for these two choices. The coordinates of the anions at equipoint 32e are not special: they vary according to a single parameter, *u*. For a perfect ccp anion arrangement, $u^{\bar{4}3m}_{\text{ideal}} = ⅜$ (0.375) and $u^{\bar{3}m}_{\text{ideal}} = ¼$ (0.250), for origins at $\bar{4}3m$ and $\bar{3}m$, respectively.

Figure 2 shows the spinel-crystal lattice arrangement for layers along the [001] crystallographic axis, at intervals of one-eighth of the unit-cell dimension (*a*/8). The origin in Fig. 2 is located at $\bar{4}3m$ on an A-site cation (the $\bar{3}m$ setting on an octahedral vacancy is obtained when all the lattice sites are translated by the vector [$-⅛a$,$-⅛a$,$-⅛a$]). Anions are shown at their ideal locations in Fig. 2; the arrows indicate the translations that are defined by the generalized anion position parameter, *u*. Anions in spinel usually are dilated away from their ideal ccp positions. This dilation has several important crystallographic implications, which include changes in bond lengths, bond angles, interstice volumes, and the symmetries of coordination polyhedra.

Table III shows the dependence of certain lattice distances on the anion parameter *u* and the lattice parameter *a*. The first entries in Table III are arranged according to increasing nearest-neighbor distances, relative to A-site and B-site cations. The expressions in Table III, normalized with respect to *a*, are plotted in Fig. 3. Many lattice distances are identical in the ideal spinel ccp structure ($u^{\bar{4}3m}_{\text{ideal}} = 0.375$; $u^{\bar{3}m}_{\text{ideal}} = 0.250$) but become degenerate upon anion-lattice dilation.

The lattice distances between the cations and the neighboring vacancies that are shown in Table III and Fig. 3 have important consequences, in regard to self-diffusion in spinels. For instance, a B-site cation that makes a diffusion jump to a nearest-neighbor vacant octahedral site (16c; multiplicity of 6) can move directly to the octahedral vacancy or migrate via a first-nearest-neighbor vacant tetrahedral site (8b or 48f; multiplicity of 8). For ideal ccp anion packing, the latter route should be preferred, because the former involves moving neighboring anions.[8] But for $u^{\bar{4}3m} > 0.385$, competition between the two routes can be expected.[9] For tetrahedral A-sites, a diffusion jump to a nearest-neighbor tetrahedral vacant site (48f; multiplicity of 6) can occur by a direct jump or by migration via a nearest-neighbor vacant octahedral site (16c; multiplicity of 4). Again, the latter route should be preferred, except in compounds with large *u* values.[9]

Table IV shows relationships between polyhedral volumes (*V*) in spinel and parameters *u* and *a*. The expressions for *V* from Table IV, normalized with respect to the unit-cell volume ($V_{\text{u.c.}} = a^3$) are plotted in Fig. 4. As with bond lengths, the volumes of the various tetrahedral coordination polyhedra converge at $u^{\bar{4}3m}_{\text{ideal}} = 0.375$ ($u^{\bar{3}m}_{\text{ideal}} = 0.250$) (likewise for octahedral polyhedra). Figure 5 shows schematic diagrams for the coordination polyhedra from Table IV and Fig. 4. The nearest-neighbor environment for each lattice site in Fig. 5 is shown for ideal ccp spinel. Anion displacement vectors also are indicated in Fig. 5(a), to show the effect of anion-sublattice dilation on the tetrahedral A-site.

As *u* increases from its ideal value, anions move away from the tetrahedrally coordinated A-site cations along the ⟨111⟩ directions, which increases the volume of each A-site interstice while the octahedral B-sites become correspondingly smaller. For a given binary spinel compound, the anion sublattice expands or contracts by varying *u*, until the A- and B-site volumes match the radii of the constituent cations. The symmetry of the regular tetrahedra that are associated with A-sites ($\bar{4}3m$) is unchanged by the anion-lattice dilation; however, B-sites suffer reduced symmetry ($\bar{3}m$ rather than $m\bar{3}m$ regular octahedra). Changes in site symmetries with anion dilation are reflected in bond-angle variations with *u*. This relation is illustrated in Fig. 6 for several interbond angles between the cations and anions. These structural variations have important implications for materials properties. For instance, the angle A-X-B (in ideal ccp, 125.264°) shown in Fig. 6 is the coupling angle for the primary superexchange interaction in ferrimagnetic oxide spinels.[10]

A-site tetrahedra in spinel are isolated from each other and

Table II. Fractional Coordinates of Lattice Sites in the Cubic Unit Cell of Spinel

Lattice site	Equipoint†	Point symmetry	Fractional coordinates of lattice sites: Origin on $\bar{4}3m$ at A-site cation (⅛,⅛,⅛ from $\bar{3}m$ on octahedral vacancy) (0,0,0; 0,½,½; ½,0,½; ½,½,0)+	Fractional coordinates of lattice sites: Origin on inversion center $\bar{3}m$ at octahedral vacancy (−⅛,−⅛,−⅛ from $\bar{4}3m$ on A-site cation) (0,0,0; 0,½,½; ½,0,½; ½,½,0)+
A-site cation	8a	$\bar{4}3m$	0,0,0; ¼,¼,¼	⅛,⅛,⅛; ⅞,⅞,⅞
Tetrahedral vacancy	8b	$\bar{4}3m$	½,½,½; ¾,¾,¾	⅜,⅜,⅜; ⅝,⅝,⅝
B-site cation	16d	$\bar{3}m$	⅝,⅝,⅝; ⅝,⅞,⅞; ⅞,⅝,⅞; ⅞,⅞,⅝	½,½,½; ½,¼,¼; ¼,½,¼; ¼,¼,½
Octahedral vacancy	16c	$\bar{3}m$	⅛,⅛,⅛; ⅛,⅜,⅜; ⅜,⅛,⅜; ⅜,⅜,⅛	0,0,0; 0,¼,¼; ¼,0,¼; ¼,¼,0
Anion X	32e	3*m*	*u*,*u*,*u*; *u*,$\bar{u}$,$\bar{u}$; $\bar{u}$,*u*,$\bar{u}$; $\bar{u}$,$\bar{u}$,*u*; (¼ − *u*),(¼ − *u*),(¼ − *u*); (¼ + *u*),(¼ + *u*),(¼ − *u*); (¼ + *u*),(¼ − *u*),(¼ + *u*); (¼ − *u*),(¼ + *u*),(¼ + *u*)	*u*,*u*,*u*; $\bar{u}$,$\bar{u}$,$\bar{u}$; *u*,(¼ − *u*),(¼ − *u*); (¼ − *u*),*u*,(¼ − *u*); (¼ − *u*),(¼ − *u*),*u*; $\bar{u}$,(¾ + *u*),(¾ + *u*); (¾ + *u*),$\bar{u}$,(¾ + *u*); (¾ + *u*),(¾ + *u*),$\bar{u}$
Tetrahedral vacancy‡	48f	*mm*	¼,0,0; 0,¼,0; 0,0,¼; −¼,0,0; 0,−¼,0; 0,0,−¼; ½,¼,¼; ¼,½,¼; ¼,¼,½; 0,¼,¼; ¼,0,¼; ¼,¼,0	⅜,⅛,⅛; ⅛,⅜,⅛; ⅛,⅛,⅜; −⅜,⅞,⅞; ⅞,−⅜,⅞; ⅞,⅞,−⅜; −⅛,⅛,⅛; ⅛,−⅛,⅛; ⅛,⅛,−⅛; ⅛,⅞,⅞; ⅞,⅛,⅞; ⅞,⅞,⅛

†Wycoff notation. ‡For spinel, the general coordinate for the 48f site (*x*), specified in the International Tables,[4] is given by $x(\bar{4}3m) = ¼$ or $x(\bar{3}m) = ⅜$.

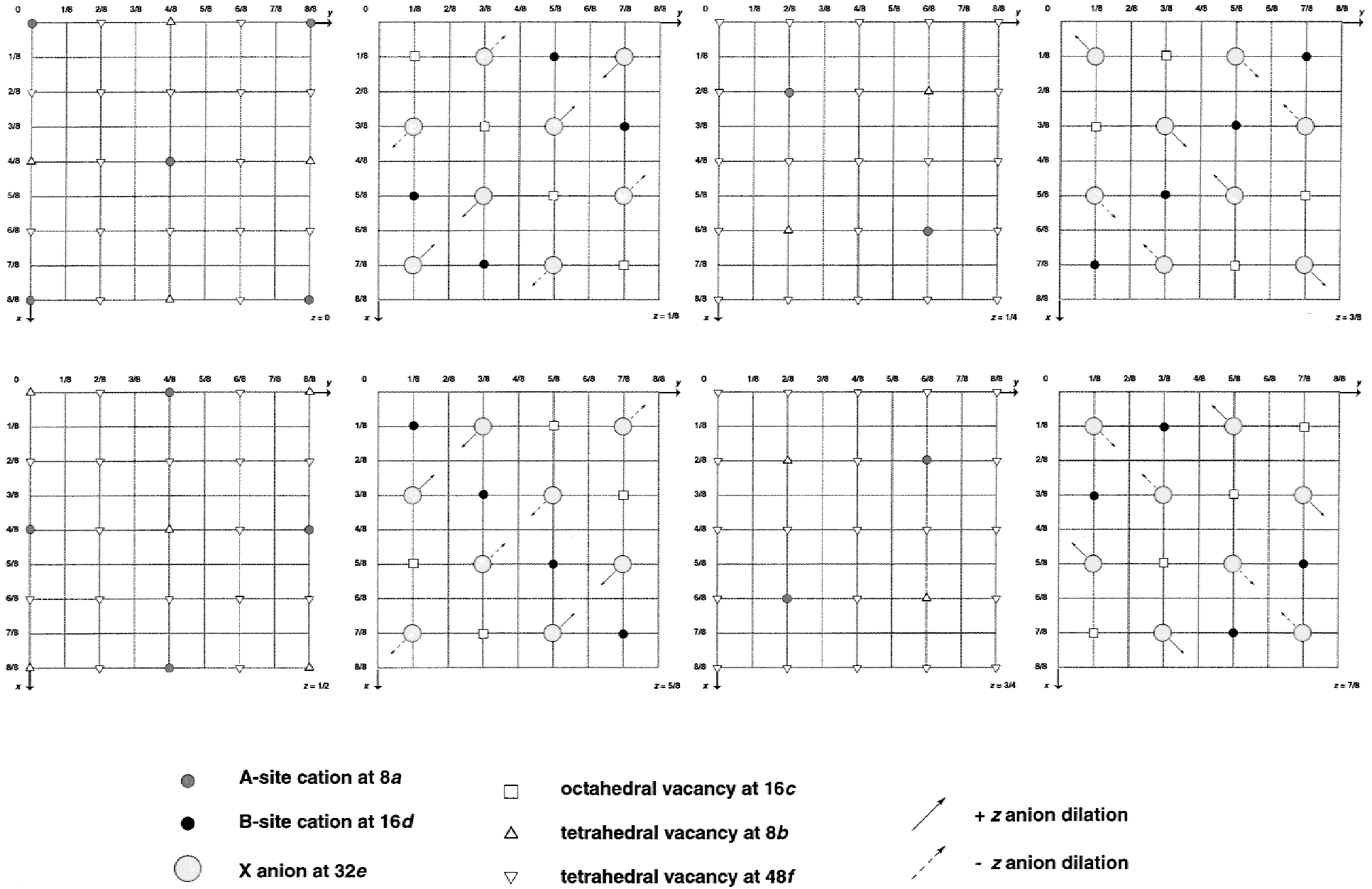

Fig. 2. Lattice sites in spinel, as a function of height along the [001] cubic cell axis. Layer sequence is shown at intervals of *a*/8. Solid arrows denote anion sublattice dilations along +*z*; dashed arrows indicate dilations along –*z*.

Table III. Spinel Bond Lengths and Selected Lattice Distances, as a Function of Anion Parameter (u) and Lattice Parameter (a)†

Species pair‡	Distance between lattice species	Coordination number§
A_{8a}–X_{32e}	$\sqrt{3}a(u - \frac{1}{4})$ (ideal ccp = $(\sqrt{3}/8)a$ = 0.216506a)	4
A_{8a}–$\square_{16c}$	$(\sqrt{3}/8)a$ = 0.216506a	4
A_{8a}–Δ_{48f}	$(1/4)a$ = 0.2500a	6
A_{8a}–$\Delta_{48f}^{2nd\ n.n.}$	$(\sqrt{2}/4)a$ = 0.353553a	12
A_{8a}–B_{16d}	$(\sqrt{11}/8)a$ = 0.414578a	12
A_{8a}–A_{8a}	$(\sqrt{3}/4)a$ = 0.433013a	4
A_{8a}–Δ_{8b}	$(\sqrt{3}/4)a$ = 0.433013a	4
B_{16d}–$\Delta_{8b,48f}$	$(\sqrt{3}/8)a$ = 0.216506a	8 (2 are 8b, 6 are 48f)
B_{16d}–X_{32e}	$a[2(u - \frac{3}{8})^2 + (\frac{5}{8} - u)^2]^{1/2}$ (ideal ccp = $\frac{1}{4}a$ = 0.2500a)	6
B_{16d}–B_{16d}	$(\sqrt{2}/4)a$ = 0.353553a	6
B_{16d}–$\square_{16c}$	$(\sqrt{2}/4)a$ = 0.353553a	6
B_{16d}–Δ_{8b}	$(\sqrt{11}/8)a$ = 0.414578a	6
B_{16d}–$\Delta_{48f}^{2nd\ n.n.}$	$(\sqrt{11}/8)a$ = 0.414578a	12
$(X_{32e}$–$X_{32e})_1$ ("unshared" anions)¶	$2\sqrt{2}a[u - \frac{1}{4}]$ (ideal ccp = $(\sqrt{2}/4)a$ = 0.353553a	3
$(X_{32e}$–$X_{32e})_2$ ("shared" anions)¶	$2\sqrt{2}a[\frac{1}{2} - u]$ (ideal ccp = $(\sqrt{2}/4)a$ = 0.353553a)	3
$(X_{32e}$–$X_{32e})_3$	$2a\{[u - \frac{3}{8}]^2 + \frac{1}{32}\}^{1/2}$ (ideal ccp = $(\sqrt{2}/4)a$ = 0.3535	6
Δ_{8b}–X_{32e}	$\sqrt{3}a[\frac{1}{2} - u]$ (ideal ccp = $(\sqrt{3}/8)a$ = 0.216506a)	4
$(\Delta_{48f}$–$X_{32e})_1$	$a\{2[u - \frac{1}{4}]^2 + [\frac{1}{2} - u]^2\}^{1/2}$ (ideal ccp = $(\sqrt{3}/8)a$ = 0.216506a)	4
$(\Delta_{48f}$–$X_{32e})_2$	$a\{[u - \frac{1}{4}]^2 + 2[\frac{1}{2} - u]^2\}^{1/2}$ (ideal ccp = $(\sqrt{3}/8)a$ = 0.216506a)	4
$\square_{16c}$–X_{32e}	$a\{2[u - \frac{3}{8}]^2 + [u - \frac{1}{8}]^2\}^{1/2}$ (ideal ccp = $\frac{1}{4}a$ = 0.2500a)	6

†Expressions are for origin $\bar{4}3m$ (to convert to $\bar{3}m$, replace u with $u + \frac{1}{8}$). ‡A and B are the cations, and X is the anion; "□" denotes an octahedral vacancy, and "Δ" represents a tetrahedral vacancy. §The coordination number is the number of equivalent nearest-neighbor bonds, with respect to the first species denoted in the lattice-distance expression. ¶The "unshared" anions actually are shared by two vacant octahedra (16c, 16c) and two tetrahedra (occupied 8a and vacant 48f). The "shared" anions actually are shared by two occupied octahedra (16d, 16d) and two vacant tetrahedra (8b, 48f). The remaining anions are shared by two octahedra (occupied 16d and vacant 16c) and two vacant tetrahedra (48f, 48f).

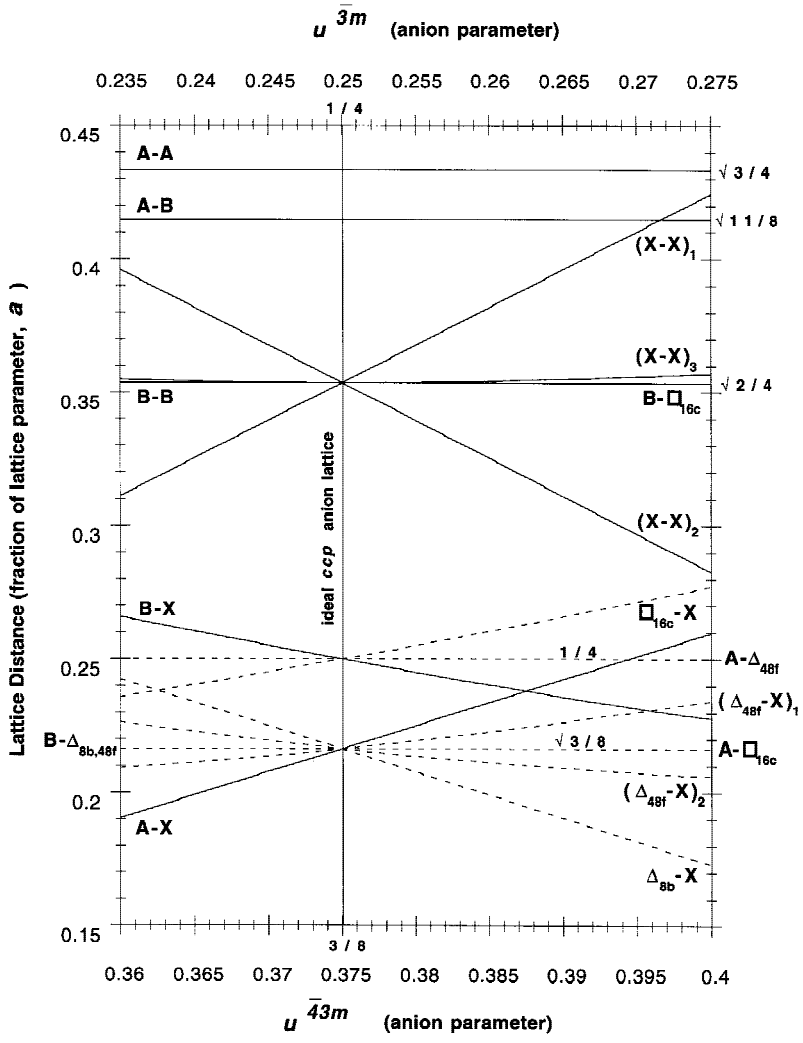

Fig. 3. Bond lengths (solid lines) and interlattice distances (dotted lines) in spinel, as a function of anion parameter u. Distances normalized to the cubic cell edge a.

Table IV. Polyhedral Volumes, *V*, in Spinel, as a Function of Anion Parameter (*u*) and Lattice Parameter (*a*)†

Polyhedral volume	Expression for polydedral volume	Polyhedron, symmetry
$V_{tet}^{A_{8a}}$	$\frac{8}{3}a^3(u - \frac{1}{4})^3$ (ideal ccp = $\frac{1}{192}a^3$ = $0.00520833a^3$)	Regular tetrahedron, $\bar{4}3m$
$V_{tet}^{A_{8b}}$	$\frac{8}{3}a^3(\frac{1}{2} - u)^3$ (ideal ccp = $\frac{1}{192}a^3$ = $0.00520833a^3$)	Regular tetrahedron, $\bar{4}3m$
$V_{tet}^{A_{48f}}$	$\frac{1}{3}a^3(\frac{1}{2} - u)(u - \frac{1}{4})$ (ideal ccp = $\frac{1}{192}a^3$ = $0.00520833a^3$)	Irregular tetrahedron, $mm2$ (ideal ccp = regular tetrahedron, $\bar{4}3m$)
$V_{oct}^{B_{16d}}$	$16\frac{2}{3}a^3(\frac{1}{2} - u)^2(u - \frac{1}{8})$ (ideal ccp = $\frac{1}{48}a^3$ = $0.02083333a^3$)	Irregular octahedron, $\bar{3}m$ (ideal ccp = regular octahedron, $m\bar{3}m$)
$V_{oct}^{B_{16c}}$	$16\frac{2}{3}a^3(u - \frac{1}{4})^2(\frac{5}{8} - u)$ (ideal ccp = $\frac{1}{48}a^3$ = $0.02083333a^3$)	Irregular octahedron, $\bar{3}m$ (ideal ccp = regular octahedron, $m\bar{3}m$)
$V_{oct}^{X_{32e}}$	$\frac{1}{192}a^3$ = $0.00520833a^3$	Irregular tetrahedron, $mm2$

†Expressions are for origin $\bar{4}3m$ (to convert to $\bar{3}m$, replace u with $u + \frac{1}{8}$).

share corners with neighboring B-site octahedra. No edge sharing occurs between A-site tetrahedra and other A- or B-site polyhedra. B-site octahedra share six of twelve X-X edges with nearest-neighbor B-site octahedra. The other six edges are shared with octahedra that surround 16c vacant sites. The X-X edges that are shared by the B cations form chains in the lattice along the ⟨110⟩ directions. Because no intervening anions obstruct neighboring B-site cations, B-B distances are short (Fig. 3), which facilitates electrical conductivity in some spinels, via electron hopping between B-sites.[11,12]

III. Cation Arrangements

Barth and Posjnak[13–15] were the first to note that many compounds that exhibit the spinel structure can accommodate sig-

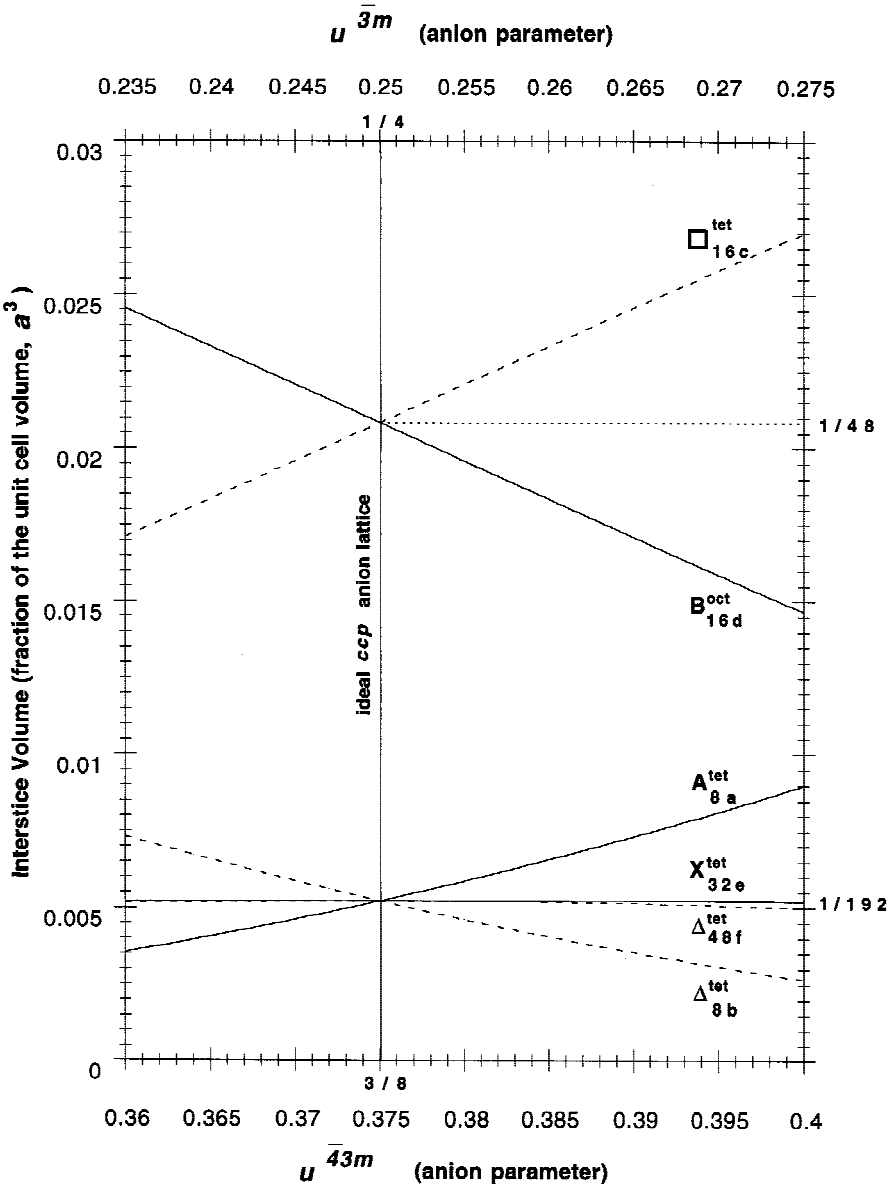

Fig. 4. Interstice volumes for atomic sites (solid lines) and interstitial sites (dotted lines), as a function of anion parameter *u*. Volumes normalized to the cubic cell volume a^3.

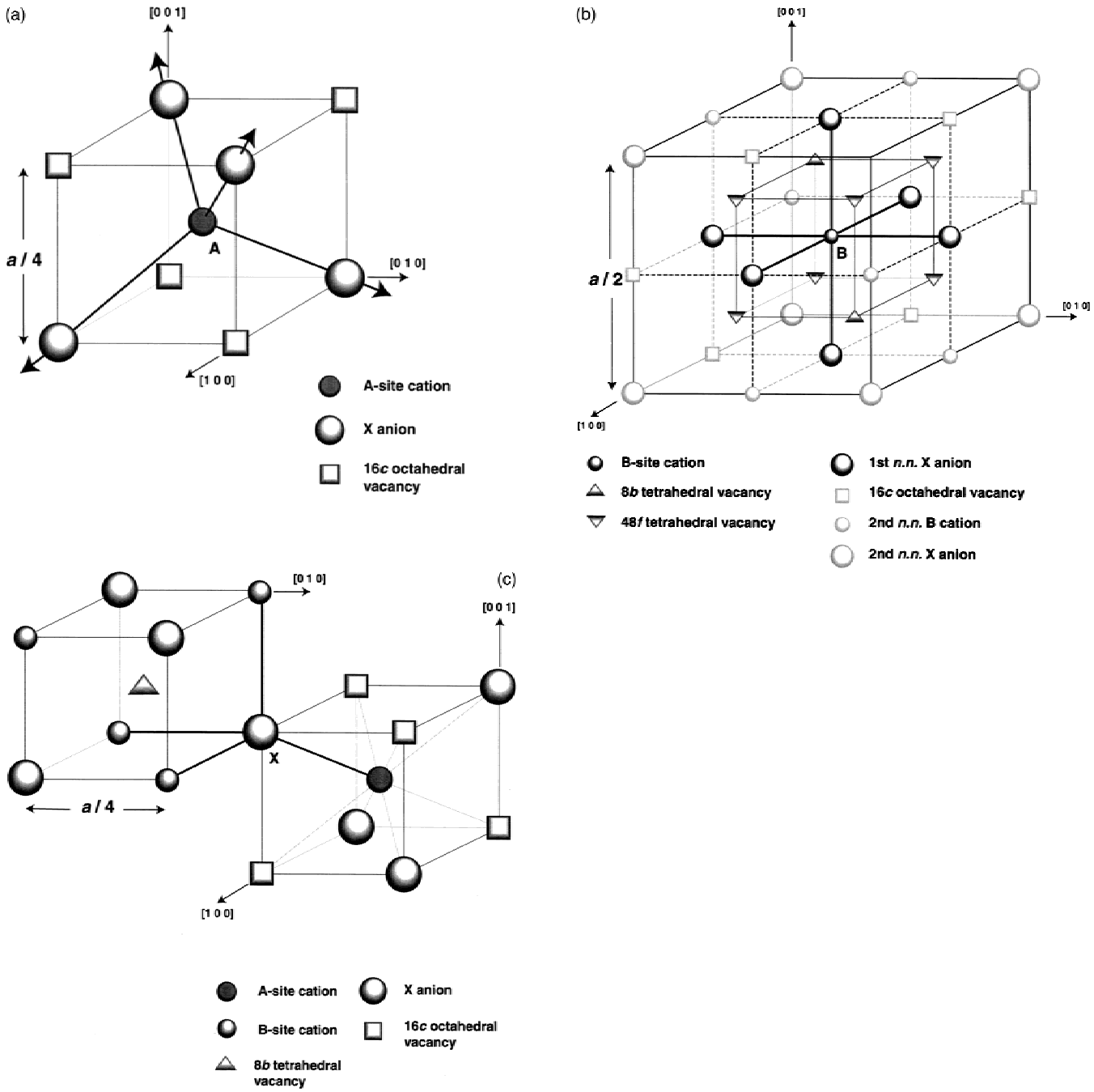

Fig. 5. Schematic drawings of lattice surroundings and nearest neighbors for (a) the tetrahedral A-site (8a), (b) the octahedral B-site (16d), and (c) the tetrahedral anion X-site (32e). Anion dilations are indicated in Fig. 5(a) by solid arrows.

nificant amounts of cation disorder, at so-called "variate atom equipoints." Verwey and Heilmann[16] introduced the designations "normal spinel" and "inversed spinel" for the limiting configurations of cations in spinel-structured compounds. In a "normal" 2-3 spinel ($MgAl_2O_4$, for instance), where "2" and "3" refer to a compound that is composed of divalent and trivalent cations, the divalent minority cations (Mg^{2+}) occupy tetrahedral A-sites, whereas the trivalent majority cations (Al^{3+}) reside in octahedral B-sites. In an "inverse" 4-2 spinel (e.g., qandilite, $TiMg_2O_4$), where "4" and "2" refer to a spinel that is composed of quadravalent and divalent cations, the A-sites are filled entirely by divalent majority cations (Mg^{2+}), whereas the B-sites are occupied by divalent majority (Mg^{2+}) and quadravalent minority (Ti^{4+}) cations, in equal proportions.

Experiments reveal that cation order often is located somewhere between the extremes of normal and inverse spinel. The structural formula for a binary spinel with composition $M(1)M(2)_2X_4$ may be written as follows:

$$[M(2)_i^{q+}M(1)_{1-i}^{p+}]^{A_{IV}}[M(1)_{i/2}^{p+}M(2)_{(2-i)/2}^{q+}]_2^{B_{VI}}X_4$$

where $M(1)^{p+}$ and $M(2)^{q+}$ are minority and majority cations, respectively. The first quantity in brackets represents the average occupancy of A-sites (coordination number of four (IV)), whereas the second quantity in brackets represents the average occupancy of B-sites (coordination number of six (VI)). The variable i is the so-called inversion parameter, which specifies the fraction of A-sites occupied by majority ions. For normal spinel, $i = 0$; for random cation arrangement, $i = \frac{2}{3}$, and for inverse spinel, $i = 1$. Naturally grown $MgAl_2O_4$ spinels exhibit approximately the normal spinel structure, so that $i \approx 0$; the same samples annealed at elevated temperature for a few minutes suffer cation inversion as high as $i = 0.3$.[17] It has been

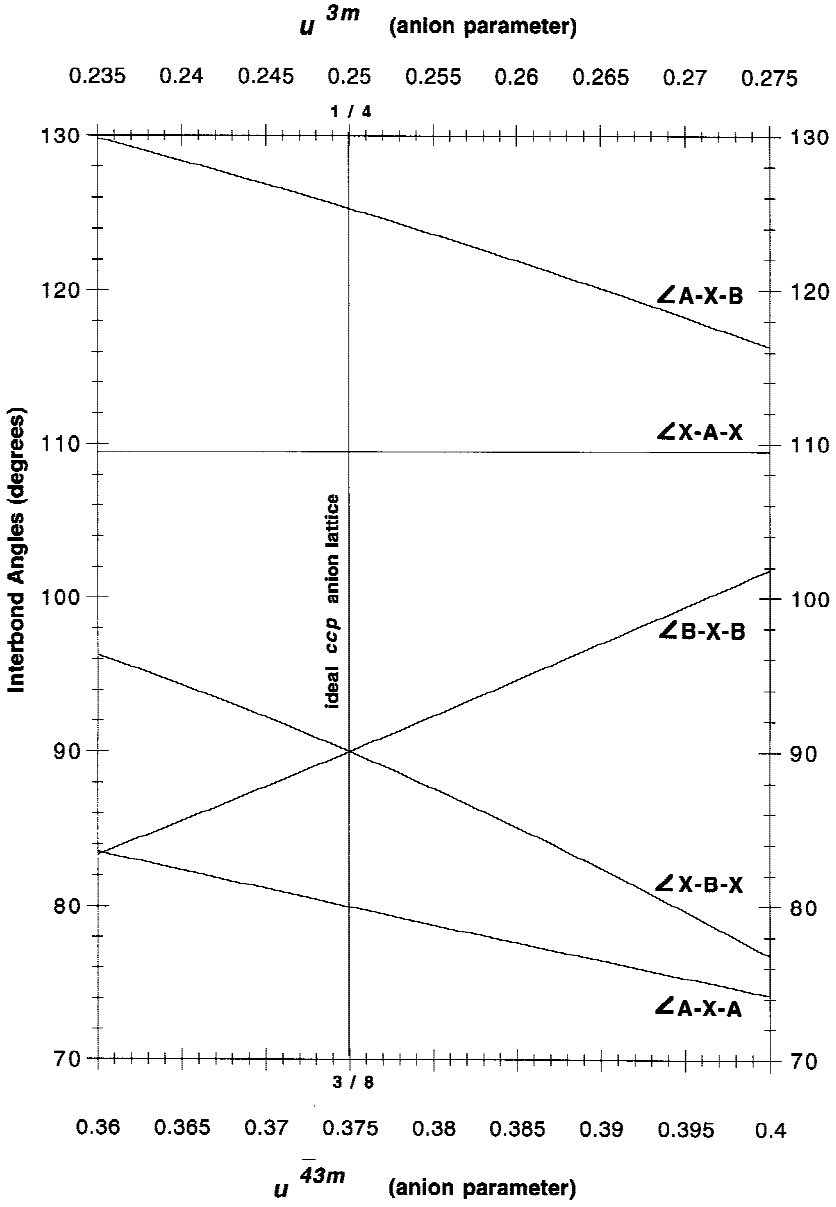

Fig. 6. Interbond angles as a function of anion parameter *u*. Bond angles are independent of *a*.

demonstrated that synthetic $MgAl_2O_4$ is always partially inverse (see, for example, Brun *et al.*[18]); inversion values of ~0.1–0.6 have been observed, the latter representing an almost-random cation arrangement.[19,20] By comparison, in the 2-3 spinel magnesioferrite, $MgFe_2O_4$, $i \approx 0.9$ in the most highly ordered material (i.e., almost inverse) but can deviate with thermal treatment to ~0.72, which, again, is an almost-random configuration (see, for example, O'Neill *et al.*[21]).

The degree of inversion (*i*) has been measured in $MgAl_2O_4$ using infrared (IR) absorption,[22,23] nuclear magnetic resonance (NMR),[24,25] magic-angle-spinning NMR (MAS-NMR),[26,27] electron spin/paramagnetic resonance (ESR/EPR),[17,20] and neutron diffraction.[19,28,29] In other spinel compounds, such as the ferrites, several additional techniques are applicable to the determination of *i*, including electrical conductivity,[30] thermopower,[31] magnetometry,[32,33] X-ray diffractometry,[21,34] and Mössbauer spectroscopy.[21]

Cation arrangements are not unique in spinels. Each spinel compound possesses at least three degrees of freedom, which it uses in its search for an equilibrium structure: *u*, *a*, and *i*. The parameter *u* varies, primarily, in accordance with the radius *ratio* between the A- and B-site cations, $r(A)/r(B)$ (or $r(B)/r(A)$). That is to say, the A- and B-site bond lengths adjust themselves by variations in *u* until the A- and B-site volumes "best-fit" the cations. The parameter *a* varies in accordance with the *average* of the A- and B-site cationic radii (i.e., with $0.33r(A) + 0.67r(B)$). The entire framework of the unit cell swells or contracts to accommodate the size of the cations. The cation inversion parameter *i* varies based on a much more complex set of factors.

Some of the principal factors that influence cation inversion include[35] (i) temperature, (ii) the electrostatic contribution to the lattice energy, (iii) cationic radii, (iv) cationic charge, and (v) crystal-field effects. Thermally induced cation disorder has been described previously. Effects (ii)–(v) are considered below.

Electrostatic effects are evident upon consideration of the Madelung constant, A_M, for different lattice arrangements. Variations in A_M with spinel cation arrangement are shown in Fig. 7, based on calculations by Verwey *et al.*[36] and de Boer *et al.*,[37] using Ewald's method.[38] For inverse 2-3 and 4-2 spinels, calculations were performed two ways: (i) assuming a random distribution of cations on B-sites, and (ii) assuming an ordered cation distribution on B-sites. Ordered B-site sublattices occur

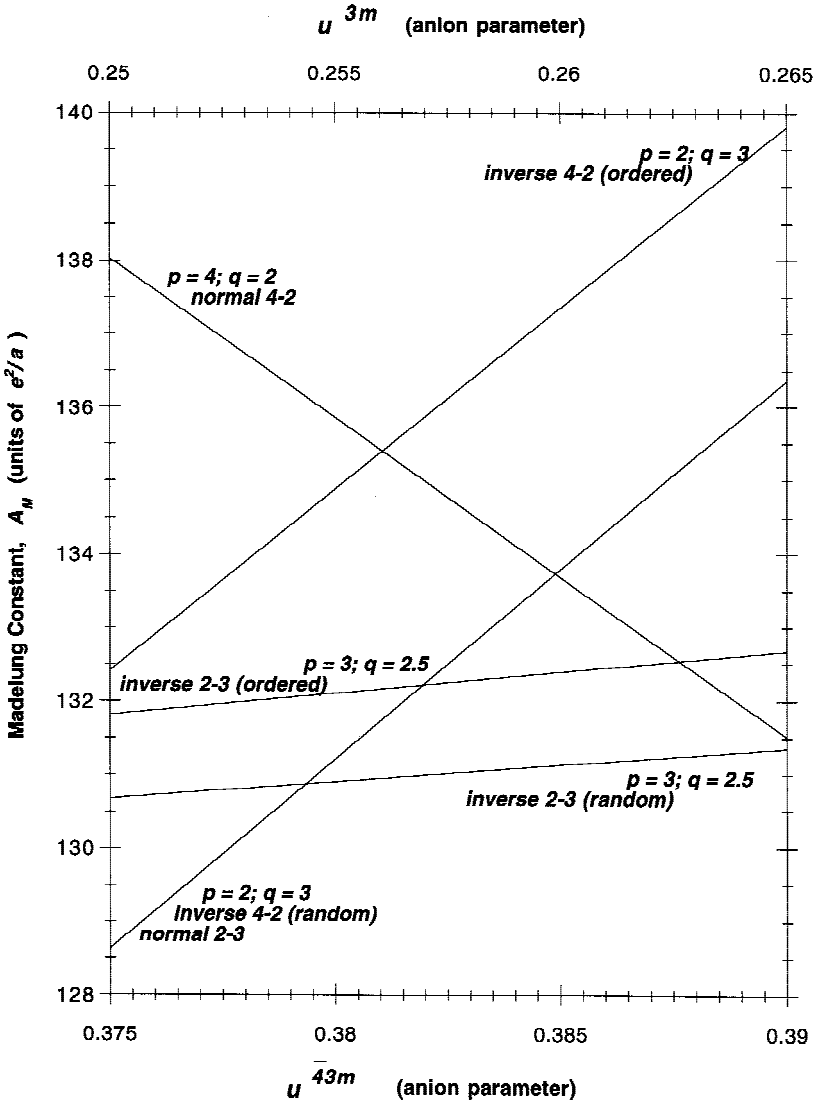

Fig. 7. Madelung constant (A_M) versus anion parameter (u) for various cation arrangements in 2-3 and 4-2 spinels. Variables p and q refer to the average charge of the cations occupying the A- and B-sites, for the different cation configurations. Data from Verwey *et al.*[36] and de Boer *et al.*[37] ($e^2 = 1.4398 \times 10^{-13}$ MeV·cm (cgs units)).

in some spinels (e.g., magnetite, $[Fe^{3+}]^A[Fe^{2+}Fe^{3+}]^BO_4$,[39] and lithium ferrite, $[Fe^{3+}]^A[Li^+_{0.5}Fe^{3+}_{1.5}]^BO_4$[40]). Figure 7 shows that, for $u^{\bar{4}3m} > 0.379$ (in the case of disordered B-sites) or $u^{\bar{4}3m} > 0.381$ (for ordered B-sites), normal spinels have greater electrostatic potential and, therefore, are more stable than inverse spinels. This relation is one of the principal reasons why almost all 2-3 spinels with $u^{\bar{4}3m} > 0.381$ are normal spinels. In the case of 4-2 spinels, for $u^{\bar{4}3m} > 0.381$ (ordered B-sites) or $u^{\bar{4}3m} > 0.385$ (random B-sites), the inverse structure is more stable than that of normal spinel. These calculations highlight a dramatic difference between 2-3 and 4-2 spinels: 2-3 and 4-2 spinels with similar u values have a tendency to have cation arrangements at opposing limits of inversion.

Cation radii and charge effects have a tendency to counteract each other. For instance, in a normal 2-3 spinel, cation occupancy satisfies the Verwey–Heilmann principle of maximal charge neutralization,[16] whereas, in an inverse 2-3 spinel, this principle is defied. The Verwey–Heilmann principle states "if neutralization of charge is to be sharply localized around cations, then cations of high valence will have large coordination numbers, so as to be neutralized efficiently by numerous anions in the first coordination shell." However, high-valence cations generally possess small ionic radii and, thus, according to Pauling's first rule,[41] they may be sufficiently undersized so as to "rattle" in their confining cages between anions. Pauling's rule states "as cation valence increases, small interstices and small coordination numbers become preferable." The propensity for cation disordering that is observed in spinels is, in part, a consequence of the struggle between these cross-purposes.

$MgAl_2O_4$ provides one of the best examples of cation-site competition in spinel compounds. The fact that natural spinel is a normal spinel implies that the smaller Al^{3+} cation has a thermodynamic preference for the octahedral B-site. However, calculations of the point-defect formation energies in $MgAl_2O_4$ indicate that the energy expended in the cation antisite reaction (i.e., $Mg_A + Al_B \rightarrow Al^{\bullet}_A + Mg'_B$) is smaller than that for any other point-defect formation reaction.[42] Disordering defects readily form in $MgAl_2O_4$; therefore, it comes as little surprise that all attempts to synthesize pure, fully ordered magnesium aluminate spinel crystals have failed.

Despite the voluminous literature that has been devoted to crystal-field phenomena in spinels, these effects are not as perplexing as they may seem. Basically, they may be summarized as follows. If one of the constituents of a spinel compound is a transition-metal ion, and this ion has a relatively large crystal-field stabilization energy (CFSE) (that energy being some fraction of the octahedral crystal-field splitting energy, Δ_{oct}), then this ion will compete for octahedral B-site

occupancy, even at the expense of increased electrostatic energy or other structural factors. For oxide spinels, the CFSE is easy to calculate because oxygen ions are weak-field ligands (Δ_{oct} is small). Consequently, almost all transition-metal ions in spinel obey Hund's rule and adopt high-spin (HS) configurations (see, for example, Jaffe[43]). Sc^{3+}, Ti^{4+}, Mn^{2+}, Fe^{3+}, and Zn^{2+} cations in their HS configurations exhibit no CFSE and, therefore, have no crystal-field-induced preference for B-sites. The largest CFSEs among transition-metal ions belong to Cr^{3+} and Ni^{2+} ions (CFSE = $\frac{6}{5}\Delta_{oct}$ for both ions). Of these ions, the Cr^{3+} ion exhibits the maximum propensity for B-site occupancy, and, consequently, all chromates ($M(1)Cr_2O_4$) are normal spinels. The 2-3 spinel chromite, $FeCr_2O_4$, for instance, assumes the normal cation arrangement and may be written as $[Fe^{2+}]^A[Cr^{3+},Cr^{3+}]^BO_4$.[44] In chromite, the Fe^{2+} cation is relegated to the tetrahedral A-site, even though it possesses a respectable CFSE (equal to $\frac{2}{5}\Delta_{oct}$). On the other hand, in the 2-3 spinel magnetite ($FeFe_2O_4$), the Fe^{2+} cation successfully adopts the B-site, and this spinel is an inverse spinel: $[Fe^{3+}]^A[Fe^{2+},Fe^{3+}]^BO_4$.[44] In this case, the ferric ion (Fe^{3+}), with no CFSE, relinquishes half of the octahedral sites to the ferrous species (Fe^{2+}). However, in the 2-3 iron aluminate spinel hercynite ($FeAl_2O_4$), the Fe^{2+} cation again concedes the battle for the B-site. Hercynite is a normal spinel, with a structure that is given by $[Fe^{2+}]^A[Al^{3+},Al^{3+}]^BO_4$. Despite possessing no CFSE, the Al^{3+} ion in hercynite shows a remarkable Verwey–Heilmann-like preference for the B-site. This B-site preference by the Al^{3+} ion is aided by several factors:

(1) The Fe^{2+} ion is one of the largest divalent ions found in spinels, whereas the Al^{3+} ion is the smallest of the trivalent spinel cations; thus, the $r(Fe^{2+})/r(Al^{3+})$ ratio is large, which favors large u values (the measured value for hercynite is $u^{43m} = 0.3900$[44]);

(2) According to electrostatic considerations for 2-3 spinels, large u values favor a normal spinel, i.e., Al^{3+} cations on B-sites in hercynite; and

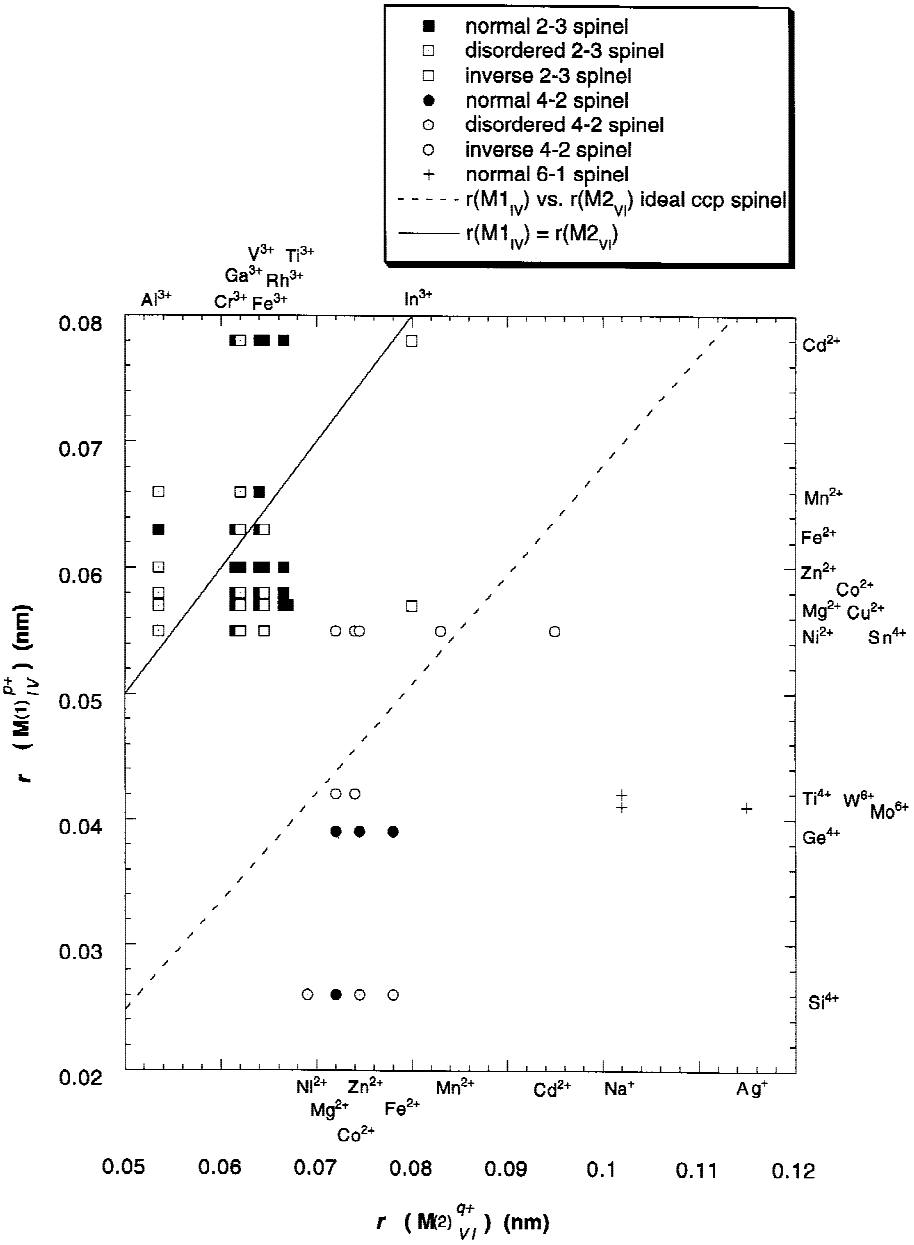

Fig. 8. Spinel-forming oxides from Table V, plotted versus effective cationic radii, ($r(M(1)^{p+}_{IV})$ and $r(M(2)^{q+}_{VI})$). These radii are appropriate for normal cation arrangements. 2-3 spinels are clustered near the line representing $r(M(1)^{p+}_{IV}) = r(M(2)^{q+}_{VI})$, whereas 4-2 spinels are more similar to the radius relationship for ideal ccp oxides, given by $r(M(1)^{p+}_{IV}) = 0.8660r(M(2)^{q+}_{VI}) - 0.185$ (in nanometers) (assuming $r(O^{2-}_{IV}) = 0.138$ nm). Ionic radii are from Shannon.[45]

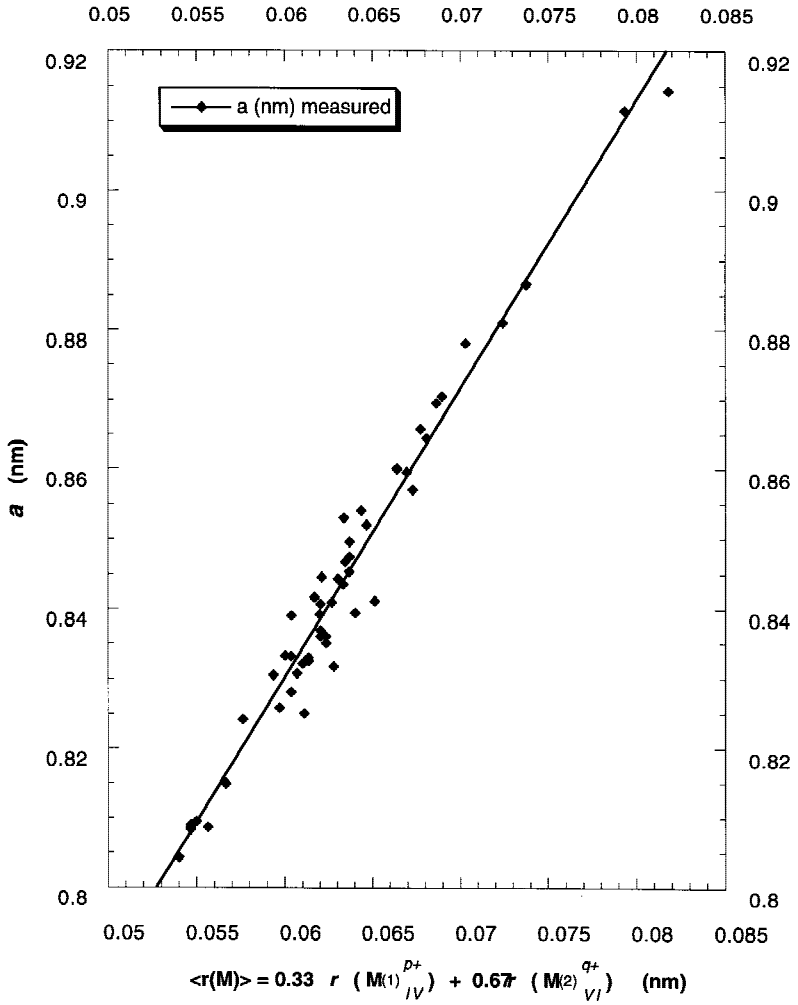

Fig. 9. Measured lattice parameter (a) versus average cation radius ($\langle r(\mathrm{M})\rangle$) for the 2-3 and 4-2 oxide spinels from Fig. 8 and Table V (high-pressure silicate 4-2 spinels were not included in this plot). $\langle r(\mathrm{M})\rangle$ is calculated assuming a normal cation distribution, and a linear least-squares fit to the data is shown as a solid line.

(3) According to Table III and Fig. 3, B−O bonds are shorter than A−O bonds for $u^{\bar{4}3m} > 0.3875$, so that, for large u values, small cations (Al^{3+} in hercynite) best fit the B-sites. All things considered, the Fe^{2+} cation finds the A-site in hercynite comfortable enough to avoid a messy confrontation with the Al^{3+} ion.

IV. Cationic Radii and the Structure of Binary Spinel Oxides

In this section, oxide spinels are used as examples to explore relationships between the cationic radii (in the hard-sphere approximation) and the spinel structural parameters u, a, and i, discussed in the previous section. Effective ionic radii, which are dependent on nearest-neighbor coordination, are taken from the widely used compilation by Shannon.[45] Table V‡ shows a list of selected binary oxide spinels, including their cation arrangements and additional structural parameters. These data were obtained from a compilation by Hill *et al.*,[44] except that for natural $MgAl_2O_4$, in which case the data were taken from Finger *et al.*[5] The list includes 2-3, 4-2, and 6-1 spinel compounds.§ Table V is arranged according to increasing average cation radius, $\langle r(\mathrm{M})\rangle$, assuming a normal cation arrangement (i.e., $\langle r(\mathrm{M})\rangle = 0.33r(\mathrm{M}(1)^{p+}_{\mathrm{IV}}) + 0.67r(\mathrm{M}(2)^{q+}_{\mathrm{VI}})$, where IV and VI represent four- and six-fold coordination, respectively. Figure 8 shows a plot of the cation combinations that produce binary spinels, along with their respective cation radii, $r(\mathrm{M}(1)^{p+}_{\mathrm{IV}})$ and $r(\mathrm{M}(2)^{q+}_{\mathrm{VI}})$ (using values from Table V and assuming a normal cation arrangement).

Figure 9 shows a plot of the measured lattice parameter a versus $\langle r(\mathrm{M})\rangle$ for 2-3 and 4-2 spinels, from the data in Table V. A good correlation between a and $\langle r(\mathrm{M})\rangle$ is observed, although no knowledge of cation arrangements was included in the evaluation of $\langle r(\mathrm{M})\rangle$. Figure 9 also shows a linear least-squares fit to the data, wherein a and $\langle r(\mathrm{M})\rangle$ are observed to closely obey the relationship

$$a(\mathrm{nm}) = 0.5815 + 4.143\,\langle r(\mathrm{M})\rangle \qquad (\chi^2 = 0.9686) \qquad (1)$$

where $\langle r(\mathrm{M})\rangle$, given in nanometers, is equal to $0.33r(\mathrm{M}(1)^{p+}_{\mathrm{IV}}) + 0.67r(\mathrm{M}(2)^{q+}_{\mathrm{VI}})$ and χ^2 is the coefficient of determination.

‡To obtain Table V for this paper, contact the Editorial Assistant at the American Ceramic Society and request Data Depository File No. ACSD-324.

§Many binary spinels contain cations that exhibit multiple oxidation states. Only a few of these spinels are included in Table V, because the valence states and radii are uncertain in multivalent spinels. Multiple valency complicates the behavior of cations and their arrangements in spinel compounds. Essentially, multiple valency provides a compound with an additional degree of freedom to use in its quest for equilibrium. Also, the incorporation of two multivalent species in one compound can enhance electrical conductivity, by providing a mechanism for conduction via electron hopping. This condition is usually the cases for inverse spinels (e.g., Fe_3O_4), where B−B bond lengths are short enough to promote electron transfer. In normal spinels, a longer A−B hop distance is involved (Table III, Fig. 3), and these spinels do not typically conduct electrons (e.g., Mn_3O_4 and Co_3O_4).[11]

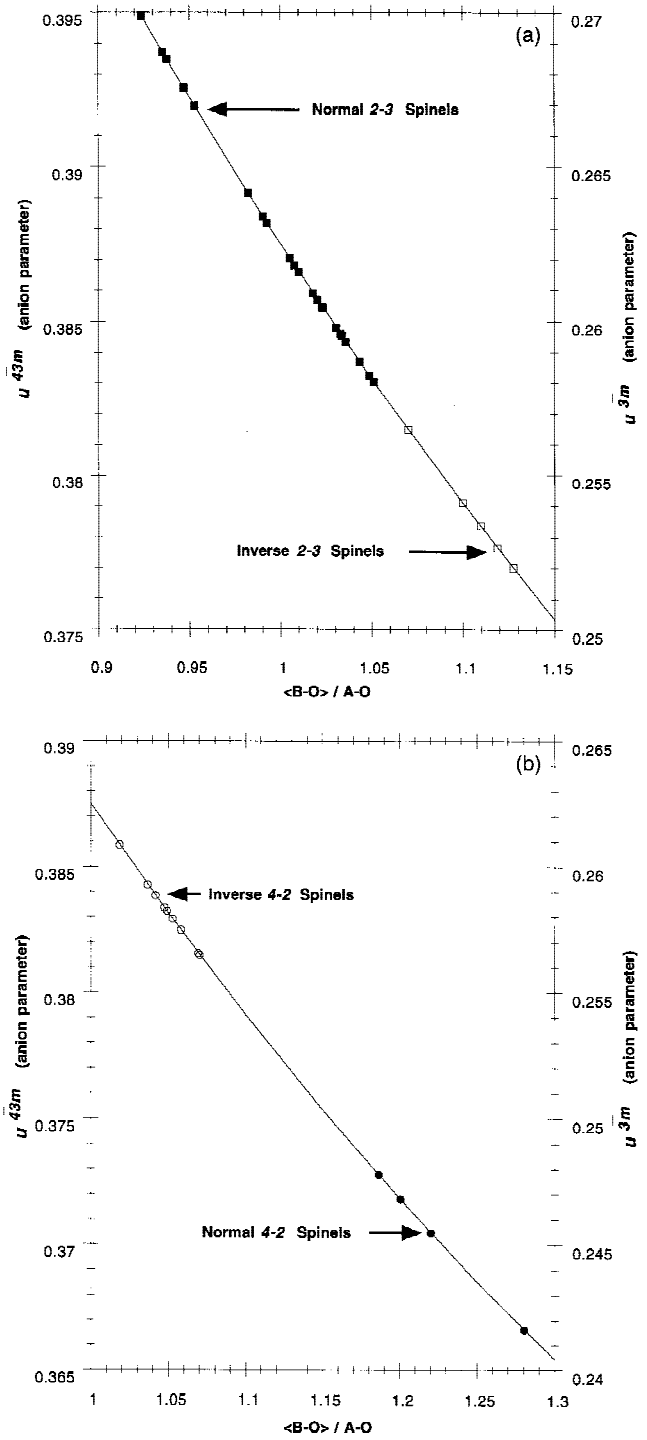

Fig. 10. Calculated anion parameter u versus $\langle$B−O$\rangle$/A−O, for (a) normal and inverse 2-3 spinel oxides and (b) normal and inverse 4-2 spinel oxides (from compounds listed in Table V). Solid curves in the figures are plots of Eqs. (2) for u versus B−O/A−O.

Figure 10 shows plots that indicate the dependence of u on the ratio of B−O to A−O bond lengths for 2-3 spinels (Fig. 10(a)) and 4-2 spinels (Fig. 10(b)). In these plots, u represents calculated values that have been obtained using the ratios of bond lengths B_{16d}−X_{32e} and A_{8a}−X_{32e} that are listed in Table III:[44]

$$u^{\bar{4}3m} = \frac{\frac{1}{2}R^2 - \frac{11}{12} + \left(\frac{11}{48}R^2 - \frac{1}{18}\right)^{1/2}}{2R^2 - 2} \qquad (2a)$$

$$u^{\bar{3}m} = \frac{\frac{1}{4}R^2 - \frac{2}{3} + \left(\frac{11}{48}R^2 - \frac{1}{18}\right)^{1/2}}{2R^2 - 2} \qquad (2b)$$

where R = B−O/A−O. Equations 2(a) and (b) are plotted in Figs. 10(a) and (b) as a solid curve. The bond lengths B−O and A−O in Fig. 10 are average bond lengths, based on the cation distributions listed in Table V; i.e., B−O = $\langle r(\mathrm{B})\rangle + r(\mathrm{O}^{2-}_{\mathrm{IV}})$ and A−O = $\langle r(\mathrm{A})\rangle + r(\mathrm{O}^{2-}_{\mathrm{IV}})$, where

$$\langle r(\mathrm{A})\rangle = ir(\mathrm{M}(2)^{q+}_{\mathrm{IV}}) + (1-i)r(\mathrm{M}(1)^{p+}_{\mathrm{IV}}) \qquad (3a)$$

$$\langle r(\mathrm{B})\rangle = \frac{i}{2}r(\mathrm{M}(1)^{p+}_{\mathrm{VI}}) + \left(\frac{2-i}{2}\right)r(\mathrm{M}(2)^{q+}_{\mathrm{VI}}) \qquad (3b)$$

and $r(\mathrm{O}^{2-}_{\mathrm{IV}})$ = 0.138 nm.[45]

Figures 11(a) and (b) show plots of u versus the cationic-radius ratio r(B)/r(A). In Fig. 11, u again represents calculated values, based on Eqs. (2). To obtain a good correlation between u and r(B)/r(A), it is necessary to invoke knowledge of the cation distributions using Eqs. (3) and i values from Table V, as shown in Fig. 11(a). If cationic radii that are based on a normal-spinel cation distribution are used, as in Fig. 11(b) (i.e., r(A) = $r(\mathrm{M}(1)^{p+}_{\mathrm{IV}})$ and r(B) = $r(\mathrm{M}(2)^{q+}_{\mathrm{VI}})$), no correlation between u and r(B)/r(A) is observed. This result illustrates the fact that the anion parameter u is very dependent on the arrangement of cations in spinel. The solid curve in Figs. 11(a) and (b) is a least-squares-power-law fit to the data in Fig. 11(a), given by

$$u^{\bar{4}3m}(\text{calculated}) = 0.3876\left(\frac{\langle r(\mathrm{B})\rangle}{\langle r(\mathrm{A})\rangle}\right)^{-0.07054} \qquad (\chi^2 = 0.9944) \qquad (4)$$

where $\langle r(\mathrm{B})\rangle$ and $\langle r(\mathrm{A})\rangle$ are calculated using Eqs. (3) and χ^2 is the coefficient of determination.

V. Additional Structure Considerations

In earlier discussions, it was implicitly assumed that B-site cations occupy positions at the exact center (center of gravity) of the octahedral B-atom interstices. This observation is not necessarily the case in all spinels. In the normal-spinel series $[Mg^{2+}]^{A}[Cr^{3+}_{x},Al^{3+}_{2-x}]^{B}O_4$, for instance, it was demonstrated, using optical fluorescence, that the Cr^{3+} ion occupies a site of 3m point symmetry,[46] rather than $\bar{3}m$ (Table II). Here, the Cr^{3+} ion is displaced from a centrosymmetric position to a noncentrosymmetric position, as a consequence of local potential conditions at the octahedral site.[47] Such displacements of B-site cations are illustrated schematically in Fig. 12. This alteration in the B-atom sublattice produces a new structure symmetry, $F\bar{4}3m$, rather than $Fd3m$. Moreover, new properties are expected for spinel structures with this reduced symmetry, such as antiferroelectricity.[48,49] In spinels where magnetic ions occupy the B-sites, the noncentrosymmetrical structure should possess unusual magnetostrictive properties and automatic enhancement of biquadratic exchange.[50]

The scientific literature is overrun with debate regarding the centrosymmetric versus noncentrosymmetric nature of spinel structures, especially for the mineral compound $MgAl_2O_4$.[51–58] The commonality of the occurrence of noncentrosymmetry in spinels is not yet clear. Strong cases have been made for $F\bar{4}3m$ symmetry in the inverse spinel magnetite ($[Fe^{3+}]^{A}[Fe^{2+}, Fe^{3+}]^{B}O_4$)[59] and the normal spinel franklinite, ($[Zn^{2+}]^{A}[Fe^{3+},Fe^{3+}]^{B}O_4$).[60–63] However, other metallic spinels, such as the strongly coupled superconductor $CuRh_2Se_4$, seem to conform to $Fd3m$ symmetry.[64,65]

In regard to the symmetry of spinel, it is interesting to consider the results of recent electronic structure calculations for the compounds $MgAl_2O_4$, $MgGa_2O_4$, and $MgIn_2O_4$. These calculations, based on density functional theory (DFT),[66] used an all-electron, full-potential electronic-structure method that was

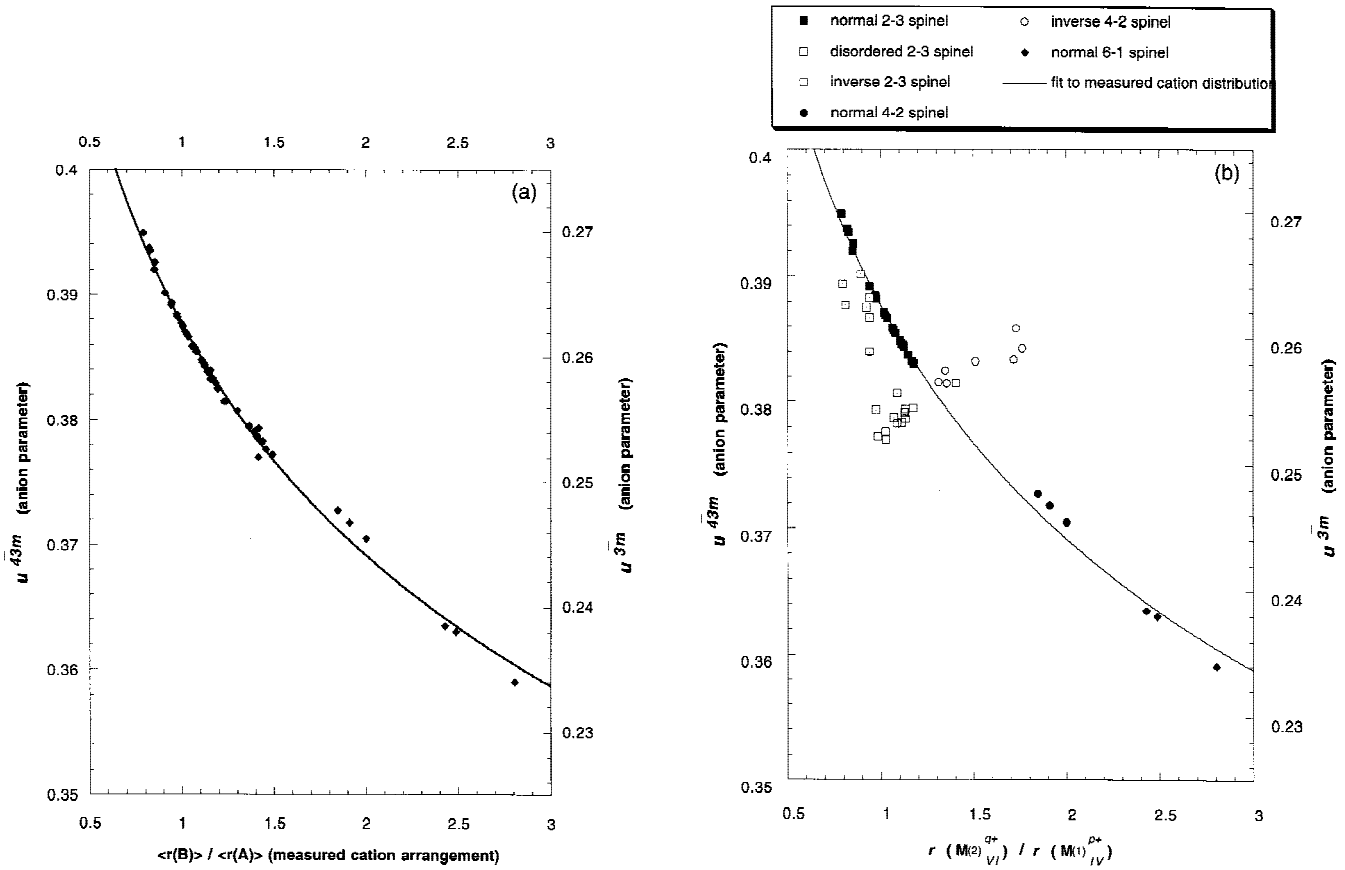

Fig. 11. Calculated anion parameter u versus (a) $\langle r(\mathrm{B})\rangle/\langle r(\mathrm{A})\rangle$ (using the measured cation arrangement) and (b) $r(\mathrm{M}(2)^{q+}_{\mathrm{VI}})/r(\mathrm{M}(1)^{p+}_{\mathrm{IV}})$ (i.e., assuming a normal cation arrangement), for spinel oxides from Table V (high-pressure silicate 4-2 spinels were not included in these plots). Solid lines in the figures represent a least-squares power-law fit to the data plotted in Fig. 11(a).

developed at Los Alamos National Laboratory,[67] which uses linear muffin-tin orbitals (LMTOs) as basis functions.[68] In calculations that are based on normal cation arrangements, a symmetry of $F\bar{4}3m$ was imposed for the starting structure of the oxides. Nevertheless, calculated spinel parameters yielded a higher symmetry for each oxide, specifically an $Fd3m$ structure. The calculations also revealed that $MgGa_2O_4$ is close to a transition to an inverse structure, whereas $MgIn_2O_4$ is an inverse structure. These results are in agreement with experiments, insofar as $MgGa_2O_4$ is disordered[69] and $MgIn_2O_4$ is

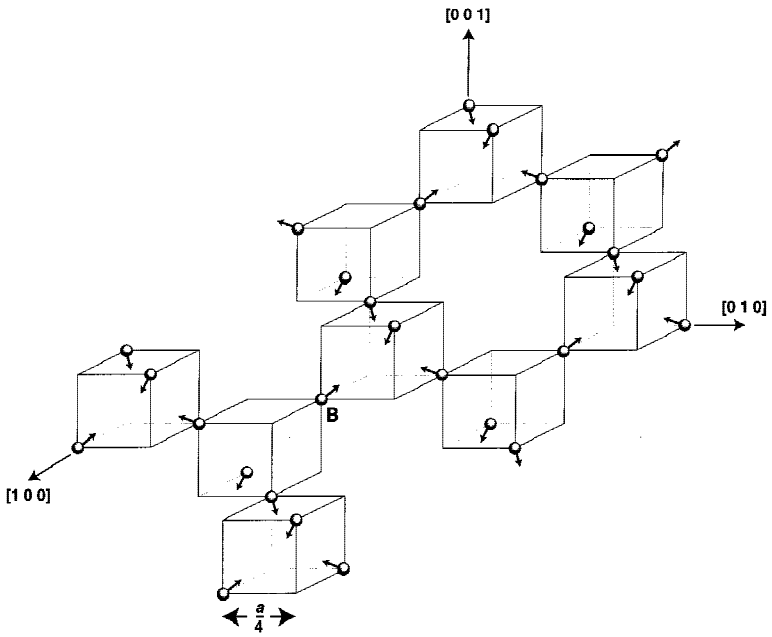

Fig. 12. Octahedral B-site cation sublattice in spinel. In some spinel compounds, a potential maximum occurs at the centers of the octahedral interstices, causing B-site cations to be displaced along the ⟨111⟩ directions (displacements are indicated by arrows).

fully inversed.[15] Calculations also were performed for inverse cation arrangements, using an imposed *Fmm*2 symmetry for the starting structures. However, once again, the calculations found a higher symmetry (the symmetry was unanalyzed) for each inverse-spinel oxide. Details of these calculations will be presented elsewhere.[70]

There are many additional symmetry and structure anomalies in spinels, which will not be discussed here. Some of these include (i) Jahn–Teller distortions in spinels that contain transition-metal ions with d^4 HS (e.g., Mn^{3+} HS) or d^9 (e.g., Cu^{2+}) electronic configurations (see, for example, Goodenough[71]); (ii) π-bond formation, which endows sulfides with metallic luster and electrical conductivity (see, for example, Jellinek[72]); and (iii) structural transformations that are induced by temperature (e.g., order–disorder transformations[73,74]), pressure (e.g., the olivine–spinel transformation[5]), chemistry,[75] or irradiation.[76]

VI. Summary

Spinel compounds possess several structural degrees of freedom that render them structurally complex but offer them extraordinary versatility. This paper has examined the role of three structural parameters that determine the detailed atomic arrangements in spinels: (i) the lattice parameter, *a*; (ii) the anion parameter, *u*; and (iii) the cation inversion parameter, *i*. Oxide spinels have been used as examples to explore the interrelationships between these parameters. In oxides, *a* is dependent on the average effective cation radius in a given compound, without significant dependence on the specific cation arrangement (*i*). On the other hand, *u* is highly dependent on *i*. This relation means that, to predict anion parameters in spinels, prior knowledge of the cation arrangements is required.

References

[1]N. W. Grimes, "The Spinels: Versatile Materials," *Phys. Technol.*, **6**, 22–27 (1975).

[2]W. H. Bragg, "The Structure of the Spinel Group of Crystals," *Philos. Mag.*, **30** [176] 305–15 (1915).

[3]S. Nishikawa, "Structure of Some Crystals of the Spinel Group," *Proc. Math. Phys. Soc. Tokyo*, **8**, 199–209 (1915).

[4]N. F. M. Henry and K. Lonsdale (eds.), *International Tables for X-ray Crystallography*, Vol. I. Kynoch Press, Birmingham, England, 1952.

[5]L. W. Finger, R. M. Hazen, and A. M. Hofmeister, "High-Pressure Crystal Chemistry of Spinel ($MgAl_2O_4$) and Magnetite (Fe_3O_4): Comparison with Silicate Spinels," *Phys. Chem. Miner.*, **13**, 215–20 (1986).

[6]F. S. Galasso, *Structure and Properties of Inorganic Solids.* Pergamon Press, Oxford, U.K., 1970.

[7]R. W. G. Wycoff, *The Analytical Expression of the Results of the Theory of Space Groups*, 2nd Ed. Carnegie Institute of Washington, Washington, DC, 1930.

[8]R. Sun, "Diffusion of Cobalt and Chromium in Chromite Spinel," *J. Chem. Phys.*, **28** [2] 290–93 (1958).

[9]N. W. Grimes, "Self-Diffusion in Compounds with Spinel Structure," *Philos. Mag.*, **25**, 67–76 (1971).

[10]S. Iida, "Layer Structures of Magnetic Oxides," *J. Phys. Soc. Jpn.*, **12** [3] 222–33 (1957).

[11]E. J. W. Verwey and J. H. de Boer, "Cation Arrangements in a Few Oxides with Crystal Structures of the Spinel Type," *Recl. Trav. Chim. Pays-Bas*, **55**, 531–40 (1936).

[12]E. J. W. Verwey, P. W. Haayman, and F. C. Romeijn, "Physical Properties and Cation Arrangement of Oxides with Spinel Structures. II. Electronic Conductivity," *J. Chem. Phys.*, **15** [4] 181–87 (1947).

[13]T. F. W. Barth and E. Posnjak, "The Spinel Structure: An Example of Variate Atom Equipoints," *J. Wash. Acad. Sci.*, **21**, 255 (1931).

[14]E. Posnjak and T. F. W. Barth, "A New Type of Crystal Fine-Structure: Lithium Ferrite ($Li_2O{\cdot}Fe_2O_3$)," *Phys. Rev.*, **38**, 2234–39 (1931).

[15]T. F. W. Barth and E. Posnjak, "Spinel Structures: With and Without Variate Atom Equipoints," *Z. Kristallogr.*, **82**, 325–41 (1932).

[16]E. J. W. Verwey and E. L. Heilmann, "Physical Properties and Cation Arrangements of Oxides with Spinel Structures. I. Cation Arrangements in Spinels," *J. Chem. Phys.*, **15** [4] 174–80 (1947).

[17]U. Schmocker, H. R. Boesch, and F. Waldner, "A Direct Determination of Cation Disorder in $MgAl_2O_4$ Spinel by ESR," *Phys. Lett.*, **40A** [3] 237–38 (1972).

[18]E. Brun, S. Hafner, P. Hartmann, and F. Laves, "Elektrische Quadrupolwechselwirkung von ^{27}Al und Kationenverteilung in Spinell ($MgAl_2O_4$)," *Naturwissenschaften*, **47**, 277 (1960).

[19]E. Stoll, P. Fischer, W. Hälg, and G. Maier, "Redetermination of the Cation Distribution of Spinel ($MgAl_2O_4$) by Means of Neutron Diffraction," *J. Phys., Paris*, **25**, 447–48 (1964).

[20]U. Schmocker and F. Waldner, "The Inversion Parameter with Respect to the Space Group of $MgAl_2O_4$ Spinels," *J. Phys. C: Solid State Phys.*, **9**, L235–L237 (1976).

[21]H. S. C. O'Neill, H. Annersten, and D. Virgo, "The Temperature Dependence of the Cation Distribution in Magnesioferrite ($MgFe_2O_4$) from Powder XRD Structural Refinements and Mössbauer Spectroscopy," *Am. Mineral.*, **77**, 725–40 (1992).

[22]S. Hafner and F. Laves, "Ordnung/Unordnung und Ultrarotabsortion III. Die Systeme $MgAl_2O_4$–Al_2O_3 und $MgAl_2O_4$–$LiAl_5O_8$," *Z. Kristallogr.*, **115**, 321–30 (1961).

[23]S. Hafner, "Ordnung/Unordnung and Ultrarotabsortion IV. Die Absorption einiger Metalloxyde mit Spinellstruktur," *Z. Kristallogr.*, **115**, 331–58 (1961).

[24]E. Brun and S. Hafner, "Die Electrische Quadrupolaufspaltung von Al^{27} in Spinell $MgAl_2O_4$ und Korund Al_2O_3. I. Paramagnetische Kernresonanz von Al^{27} und Kationenverteillung in Spinell," *Z. Kristallogr.*, **117**, 37–62 (1962).

[25]E. Brun and S. Hafner, "Die Electrische Quadrupolaufspaltung von Al^{27} in Spinell $MgAl_2O_4$ und Korund Al_2O_3. II. Das Ionenmodell zur Deutung der Gemessenen Quadrupolaufspaltung," *Z. Kristallogr.*, **117**, 63–78 (1962).

[26]G. C. Gobbi, R. Christoffersen, M. T. Otten, B. Miner, P. R. Buseck, G. J. Kennedy, and C. A. Fyfe, "Direct Determination of Cation Disorder in $MgAl_2O_4$ Spinel by High-Resolution ^{27}Al Magic-Angle-Spinning NMR Spectroscopy," *Chem. Lett.*, **6**, 771–74 (1985).

[27]R. L. Millard, R. C. Peterson, and B. K. Hunter, "Temperature Dependence of Cation Disorder in $MgAl_2O_4$ Spinel Using ^{27}Al and ^{17}O Magic-Angle-Spinning NMR," *Am. Mineral.*, **77**, 44–52 (1992).

[28]G. E. Bacon, "A Neutron Diffraction Study of Magnesium Aluminum Oxide," *Acta Crystallogr.*, **5**, 684–86 (1952).

[29]F. Fischer, "Neutronenbeugunguntersuchung der Strukturen von $MgAl_2O_4$—und $ZnAl_2O_4$—Spinellen, in Abhängigkeit von der Vorgeschichte," *Z. Kristallogr.*, **124**, 275–302 (1967).

[30]E. J. W. Verwey, P. W. Haayman, and F. C. Romeijn, "Physical Properties and Cation Arrangement of Oxides with Spinel Structures. II. Electronic Conductivity," *J. Chem. Phys.*, **15** [4] 181–87 (1947).

[31]A. Trestman-Matts, S. E. Dorris, and T. O. Mason, "Measurement and Interpretation of Thermopower in Oxides," *J. Am. Ceram. Soc.*, **66** [8] 589–92 (1983).

[32]L. Néel, "Animation à Saturation de Certains Ferrites," *Comp. R. Acad. Sci. Paris*, **230**, 190–92 (1950).

[33]R. Pauthenet, "Variation Thermique de l'Aimantation Spontanée des Ferrites de Nickel, Cobalt, Fer et Manganèse," *Comp. R. Acad. Sci. Paris*, **230**, 1842–43 (1950).

[34]E. F. Bertaut, "Sur Quelques Progrès Récents dans la Cristallography des Spinelles, en Particulier des Ferrites," *J. Phys. Radium*, **12**, 252–55 (1951).

[35]N. N. Greenwood, *Ionic Crystal Lattice Defects and Non-Stoichiometry*. Butterworths, London, U.K., 1970.

[36]E. J. W. Verwey, F. de Boer, and J. H. van Santen, "Cation Arrangements in Spinels," *J. Chem. Phys.*, **16** [12] 1091–92 (1948).

[37]F. de Boer, J. H. van Santen, and E. J. W. Verwey, "The Electrostatic Contribution to the Lattice Energy of Some Ordered Spinels," *J. Chem. Phys.*, **18** [8] 1032–34 (1950).

[38]P. P. Ewald, "Die Berechnung Optischer und Elekrostatischer Gitterpotentiale," *Ann. Phys. (Leipzig)*, **64**, 253–87 (1921).

[39]E. J. W. Verwey and P. W. Haayman, "Electronic Conductivity and Transition Point of Magnetite ('Fe_3O_4')," *Physica (Amsterdam)*, **8** [9] 979–87 (1941).

[40]P. B. Braun, "A Superstructure in Spinels," *Nature (London)*, **170**, 1123 (1952).

[41]L. Pauling, *The Nature of the Chemical Bond.* Cornell University Press, Ithaca, NY, 1960.

[42]S. P. Chen, M. Yan, J. D. Gale, R. W. Grimes, R. Devanathan, K. E. Sickafus, and M. Nastasi, "Atomistic Study of Defects, Metastable, and 'Amorphous' Structures of $MgAl_2O_4$," *Philos. Mag. Lett.*, **73** [2] 51–62 (1996).

[43]H. W. Jaffe, *Crystal Chemistry and Refractivity*. General Publishing Company, Ltd., Toronto, Ontario, Canada, 1996.

[44]R. J. Hill, J. R. Craig, and G. V. Gibbs, "Systematics of the Spinel Structure Type," *Phys. Chem. Miner.*, **4**, 317–39 (1979).

[45]R. D. Shannon, "Revised Effective Ionic Radii and Systematic Studies of Interatomic Distances in Halides and Chalcogenides," *Acta Crystallogr., Sect A: Found. Crystallogr.*, **A32**, 751–67 (1976).

[46]F. H. Lou and D. W. G. Ballentyne, "Visible and Ultra-violet Emission and Absorption Spectra of $MgAl_2O_4$:Cr," *J. Phys. C: Solid State Phys.*, **1**, 608–13 (1968).

[47]N. W. Grimes, "Structural Distortions in $MgCr_2O_4$," *J. Phys. C: Solid State Phys.*, **4**, L342–L344 (1971).

[48]N. W. Grimes, "Anti-ferroelectricity among Compounds with Spinel Structure?," *J. Phys. C.: Solid State Phys.*, **6**, L78–L79 (1973).

[49]J. Peters and K. J. Standley, "The Dielectric Behaviour of Magnesium Manganese Ferrite," *Proc. Phys. Soc., London*, **71**, 131–33 (1958).

[50]C. Kittel, "Model of Exchange-Inversion Magnetization," *Phys. Rev.*, **120**, 335–42 (1960).

[51]N. W. Grimes, "Off-Center Ions in Compounds with Spinel Structure," *Philos. Mag.*, **27**, 1217–26 (1972).

[52]L. Hwang, A. H. Heuer, and T. E. Mitchell, "On the Space Group of $MgAl_2O_4$ Spinel," *Philos. Mag.*, **21**, 241–43 (1973).

[53]E. J. Samuelson and O. Steinsvoll, "On the Space Group of Spinel," *J. Phys. C: Solid State Phys.*, **8**, L427–L429 (1975).

[54]A. H. Heuer and T. E. Mitchell, "Further Discussion on the Space Group of Spinel," *J. Phys. C: Solid State Phys.*, **8**, L541–L543 (1975).

[55]R. K. Mishra and G. Thomas, "Structural Phase Transition in the Spinel $MgAl_2O_4$," *Acta Crystallogr., Sect. A: Found. Crystallogr.*, **A33**, 678–80 (1977).
[56]P. P. K. Smith, "Note on the Space Group of Spinel Minerals," *Philos. Mag. B*, **38** [1] 99–102 (1978).
[57]M. Tokonami and H. Horiuchi, "On the Space Group of Spinel, $MgAl_2O_4$," *Acta Crystallogr., Sect. A: Found. Crystallogr.*, **A36**, 122–26 (1980).
[58]N. W. Grimes, P. Thompson, and H. F. Kay, "New Symmetry and Structure for Spinel," *Proc. Phys. Soc., London, Sect. A*, **386**, 333–45 (1983).
[59]S. Collyer, N. W. Grimes, and D. J. Vaughan, "Does Magnetite Lack a Center of Symmetry?," *J. Phys. C: Solid State Phys.*, **21**, L989–L992 (1988).
[60]A. Hudson and H. J. Whitfield, "Electric Field Gradients in Normal Spinels," *Mol. Phys.*, **12**, 165–72 (1967).
[61]B. J. Evans, S. S. Hafner, and H. P. Weber, "Electric Field Gradients at ^{57}Fe in $ZnFe_2O_4$ and $CdFe_2O_4$," *J. Chem. Phys.*, **55**, 5282–88 (1971).
[62]E. F. Westrum and D. M. Grimes, "Low Temperature Heat Capacity and Thermodynamic Properties of $ZnFe_2O_4$," *J. Phys. Chem. Solids*, **3**, 44–49 (1957).
[63]N. W. Grimes, "On the Specific Heat of Compounds with Spinel Structure. II. Zinc Ferrite," *Proc. Phys. Soc., London, Sect. A*, **338**, 223–33 (1974).
[64]P. P. Dawes, N. W. Grimes, and D. A. O'Connor, "Direct Experimental Evidence for Low Temperature Anharmonicity in Superconducting Spinels," *J. Phys. C: Solid State Phys.*, **7**, L387–L389 (1974).
[65]P. P. Dawes and N. W. Grimes, "Superconductivity among Compounds with Spinel Structure and the Strong Coupling Mechanism," *Solid State Commun.*, **16**, 139–41 (1975).
[66]P. Hohenberg and W. Kohn, "Inhomogeneous Electron Gas," *Phys. Rev.*, **136**, B864–B871 (1964).
[67]J. M. Wills and O. Eriksson, "Crystal-Structure Stabilities and Electronic Structure for the Light Actinides Th, Pa, and U," *Phys. Rev. B: Condens. Matter*, **45** [24] 13879–90 (1992).
[68]O. K. Anderson, "Linear Methods in Band Theory," *Phys. Rev. B: Condens. Matter*, **12**, 3060–83 (1975).
[69]F. Machatschki, "Der Magnesium-Gallium-Spinell," *Z. Kristallogr.*, **82**, 348–54 (1932).
[70]J. M. Wills, "Electronic Structure Calculations for Spinel Compounds: $MgAl_2O_4$, $MgGa_2O_4$, and $MgIn_2O_4$," *Phys. Rev. B: Condens. Matter*, to be submitted (1999).
[71]J. B. Goodenough, "Magnetism and Crystal Structure in Nonmetals"; pp. 1–62 in *Magnetism III: Spin Arrangements and Crystal Structure, Domains, and Micromagnetics.* Edited by G. T. Rado and H. Suhl. Academic Press, New York and London, U.K., 1963.
[72]F. Jellinek, "Sulfides"; pp. 667–748 in *Inorganic Sulfur Chemistry*. Edited by G. Nickless. Elsevier, Amsterdam, The Netherlands, 1970.
[73]C. Haas, "Phase Transitions in Crystals with the Spinel Structures," *J. Phys. Chem. Solids*, **26**, 1225–32 (1965).
[74]T. Yamanaka and Y. Takéuchi, "Order–Disorder Transition in $MgAl_2O_4$ Spinel at High Temperatures up to 1700°C," *Z. Kristallogr.*, **165**, 65–78 (1983).
[75]T. Ohzuku, A. Ueda, and N. Yamamoto, "Zero-Strain Insertion Material of $Li[Li_{1/3}Ti_{5/3}]O_4$ for Rechargeable Lithium Cells," *J. Electrochem. Soc.*, **142** [5] 1431–35 (1995).
[76]N. Yu, K. E. Sickafus, and M. Nastasi, "First Observation of Amorphization in Single-Crystal $MgAl_2O_4$ Spinel," *Philos. Mag. Lett.*, **70** [4] 235–40 (1994). □